ACS APPLIED POLYMER MATERIALS

Open Access

pubs.acs.org/acsapm

Article

Influence of Grafting Density and the Ionic Environment on the Structure of Zwitterionic Brushes

Judith Witte, Alexandros Koutsioubas, Samantha Micciulla, Laura Roxana Stingaciu, Mariano Andrés Paulin, Margarethe Dahl, Christian Fettkenhauer, Joerg Lahann, Olaf Holderer, and Stefan Wellert*

Cite This: ACS Appl. Polym. Mater. 2025, 7, 5807−5819

Read Online

ACCESS | Metrics & More | Article Recommendations | Supporting Information

ABSTRACT: Zwitterionic polymer brushes possess a high potential for applications as surface coatings, e.g., in antifouling applications. Their complex association behavior due to the coexistence of oppositely charged groups on the same monomeric unit allows for a broad variation of polarity, hydrophilicity, and the antipolyelectrolyte effect with the variation of the surrounding environment. In this study, planar polysulfobetaine brushes were investigated with neutron reflectometry (NR) and neutron spin−echo spectroscopy under grazing incidence (GINSES) to explore the brush structure and its inner dynamics perpendicular to the substrate. In particular, the effects of the substrate−initiator system and ionic strength on the structure were investigated with neutron reflectometry and a swelling by a factor of 3−5 was found in the presence of aqueous NaCl and $MgCl_2$ solutions compared to the dry state. During the data analysis, the applicability of a model-free evaluation was also demonstrated for the investigated polysulfobetaine brushes. Furthermore, it was found with GINSES that in contrast to neutral brushes, these polysulfobetaine brushes do not show the typical concentration fluctuations in the nanosecond time range when partially swollen with salt-free water.

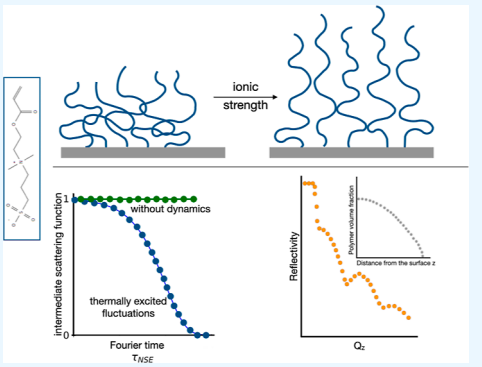

KEYWORDS: *neutron reflectometry, neutron spin - echo, grazing incidence, brushes, zwitterionic*

1. INTRODUCTION

Zwitterionic polymer brushes are formally charged, net-neutral ampholytic polymer chains that are end-tethered to a surface and contain zwitterionic groups. Methacrylate-based zwitterionic polybetaine and choline brushes are often studied in the literature. These molecules combine a positively charged entity such as a quaternary ammonium cation with a negatively charged entity such as a sulfonate (polysulfobetaine methacrylate, polySBMA), carboxylate (polycarboxybetaine methacrylate, polyCBMA), or phosphate (phosphorylcholine) anion.[1,2]

Further, the carbon spacer length (number of carbon−carbon bonds between the cationic and anionic entity) can be varied.[3] In recent years, zwitterionic polymer brushes have been extensively discussed as antifouling surface coatings.[4−8] Such coatings are important for applications like biomedical implants[9,10] and marine vessel coatings[11−14] for the prevention of biofilm formation. Hence, they can provide an important contribution to the improvement of health care and environmental sustainability. Furthermore, many zwitterionic polymers are nonthrombogenic (meaning they do not induce the formation of thrombi (blood clots), which is a serious health complication, when in contact with blood) and cell-compatible.[15] However, the selection of a suitable zwitterionic polymer brush for in vivo applications needs to combine these considerations with antifouling properties under the respective physiological conditions.

Schlenoff describes three crucial factors that contribute to the antifouling properties of zwitterions. First, zwitterions do not disrupt the H-bonding structure of water,[16] which makes them extremely hydrophilic. Second, excluded volume effects via the neutral, hydrated layer with some thickness[17] prevent protein adsorption from aqueous solution due to entropy and enthalpy penalties. Third, Schlenoff describes a gain in entropy via the release of counter ions during ion pair formation with an adsorbate as an important driving force in adsorption processes on charged surfaces. Since no release of counter ions is possible from a zwitterionic polymer brush, no entropy gain of approximately k_BT will be realized, preventing the ion pair formation with the adsorbate.[18]

The zwitterionic groups in zwitterionic polymer brushes form dipoles that result in dipole−dipole interactions between

Received: September 11, 2024
Revised: April 13, 2025
Accepted: April 25, 2025
Published: May 9, 2025

oppositely oriented dipoles and hence a self-assembly within the brush. This results in the contraction of the chains in an aqueous solution. However, the addition of salt can break these associations within the brush by shielding the charges and lead to swelling. This effect is called the antipolyelectrolyte effect because it is opposite to the polyelectrolyte effect. In the polyelectrolyte effect, the salt shields the repulsion of the same charges in the polyelectrolyte, which in case of a polyelectrolyte brush will induce collapse, while in the polyzwitterion, the salt shields the attraction between the oppositely oriented dipoles within the brush, resulting in swelling.[19,20] The effect of salt addition on the structure of different zwitterionic polymer brushes was studied by neutron reflectometry. Kobayashi et al. investigated and compared the effect of different sodium chloride concentrations on polycationic PMTAC and zwitterionic PMPC (polyphosphorylcholine) and PMAPS (polySBMA) brushes at a set grafting density and one solvent contrast.[21,22] In these measurements, it was observed for PMAPS that in D_2O, a collapsed structure forms due to the strong molecular interaction between sulfobetaine groups, while an increase of the swollen thickness in aqueous salt solution occurs. However, the dimensions of the polyphosphorylcholine brush (PMPC) did not display any dependence on salt addition. Later, Higaki et al. followed up with a similar study but adding polySBMA brushes with different carbon−carbon spacer lengths and comparing the effect of ionic strength in the surrounding environment.[2] Sakamaki et al. further investigated the effect of different salts such as sodium chloride, sodium thiocyanate, and tetramethylammonium chloride (TMAC) on thin polySBMA brushes using NR, AFM, and turbidity tests and observed a significant anion and a weak cation specificity.[23]

A parameter that is often varied in polymer brushes is the so-called grafting density. This parameter describes the number of grafted polymer chains per unit area, and in the case of grafting from procedures, it is varied during surface-initiated polymerization (SIP) by the addition of molecules with a similar chemical structure to the initiator but without the leaving group (e.g., −Br, −Cl). Huang et al. found an influence of the grafting density of a polyCBMA brush on the nonfouling properties in undiluted human serum and plasma. In the same study, they found that the dry brush thickness did not influence the fouling resistance.[24] Interestingly, another study showed that the variation of the alkyl carbon spacer length in polySBMA brushes did not affect the nonfouling properties against bacteria and fungi. However, the wetting behavior was influenced due to the changes in charge density and charge distribution.[7] Bimodal AFM studies were conducted to investigate the influence of the type of salt and salt concentration on polySBMA brushes. While the investigation showed a condensed layer toward the solid surface and a more diffuse layer toward the bulk liquid due to the influence of the salt (antipolyelectrolyte effect), the results on the influence of the type of salt and salt concentration were limited.[25] A layered structure was further described in another NR investigation where phosphocholine-based polymer brushes and polysulfobetaines (PMPC and PMAPS, respectively) were investigated. The effect of sodium chloride (up to 5.0 M) on the structure of zwitterionic polymer brushes with grafting densities of 0.1 nm^{-2} was investigated here. The rather compact brushes in salt-free D_2O swelled to a bimodal configuration in the presence of an aqueous NaCl solutions.[22,26]

In a molecular dynamics study combined with AFM experiments, Song et al. simulated the salt responsiveness of PSBMA, PCBMA, and PMPC brushes and their effect on protein adsorption. The effect of monovalent NaCl and divalent $CaCl_2$ was investigated, and it was found that the addition of NaCl reduced protein adhesion to polySBMA and polyCBMA brushes, while it was enhanced for PMPC brushes. In contrast, divalent $CaCl_2$ resulted in calcium bridges between polySBMA and polyCBMA brushes and proteins, preventing the protein from moving away from the brush surface. This was explained by the fact that monovalent cations disrupt the formation of salt bridges with proteins by shielding the charge in the brush, while divalent cations form even stronger calcium bridges between the brush and protein. Therefore, they conclude polySBMA and polyCBMA to be suitable as antifouling coatings in monovalent salt solutions, while PMPC is advantageous in divalent ones.[27]

However, up to now, the number of reports in the literature on the use of NR for structural investigations of planar polyzwitterionic brushes with both mono- and divalent salts is very limited. This is in contrast to the use of this technique for the characterization of neutral and polyelectrolyte brushes[28,29] and reports on copolymer films containing sulfobetaine units.[30,31] Hence, for this study, monovalent NaCl and divalent $MgCl_2$ were added in different concentrations to investigate their influence on the internal structure of polySBMA brushes with different grafting densities in NR experiments. Due to their comb-like molecular structure and the presence of charged molecular groups in the side chains, additional NR measurements will continue to complete the understanding of the inner structure of these brushes. That knowledge will also help, for example, to understand the influence of this structure on the ion distribution and penetration inside the brushes. Therefore, an unbiased model-free reconstruction of the polymer volume fraction profiles of the polySBMA brushes using indirect Fourier transform analysis of the data was applied.

Further, grazing incidence neutron spin echo spectroscopy (GINSES) allows studying thermal fluctuations of polymers at interfaces, e.g., neutral brushes[32] or adsorbed microgels.[33] Based on our experience with these polymer architectures, GINSES was used in this work to explore the near-surface dynamics of the zwitterionic polySBMA brushes. An example of polySBMA brushes is pMEDSAH brushes, which were investigated in this work (the abbreviation PMAPS is also frequently used in the literature). To our knowledge, this is the first investigation of any type of zwitterionic polymer brushes with grazing incidence neutron spin echo spectroscopy.

2. EXPERIMENTAL SECTION

2.1. Materials. *N*-(3-Sulfopropyl)-*N*-methacryloxyethyl-*N*,*N*-dimethylammonium Betaine (MEDSAH; >95%) was purchased from Monomer-Polymer and Dajac Laboratories and Sigma-Aldrich. 2,2′-Bipyridine (bpy, ≥99%), copper(I) chloride (≥99%), copper(II) chloride (99%), methanol (z.A. min. 99.8% CH_2OH), tetrahydrofuran (anhydrous, ≥99%, inhibitor-free), toluene (anhydrous, 99.8%), and trichlorododecylsilane (≥95%) were purchased from Sigma-Aldrich. [11-(2-Bromo-2-methyl)propionyloxy]undecyltrichlorosilane (eBMPUS, 95%) was purchased from Gelest. All of the above chemicals were used as received. Water was purified with a Milli-Q system (Millipore) with a resistance of 18 MΩ cm.

2.2. Substrate Preparation. Silicon blocks for the neutron scattering experiments were purchased from Siliciumbearbeitung Andrea Holm GmbH (Germany). For laboratory measurements, 1

https://doi.org/10.1021/acsapm.4c02879
ACS Appl. Polym. Mater. 2025, 7, 5807−5819

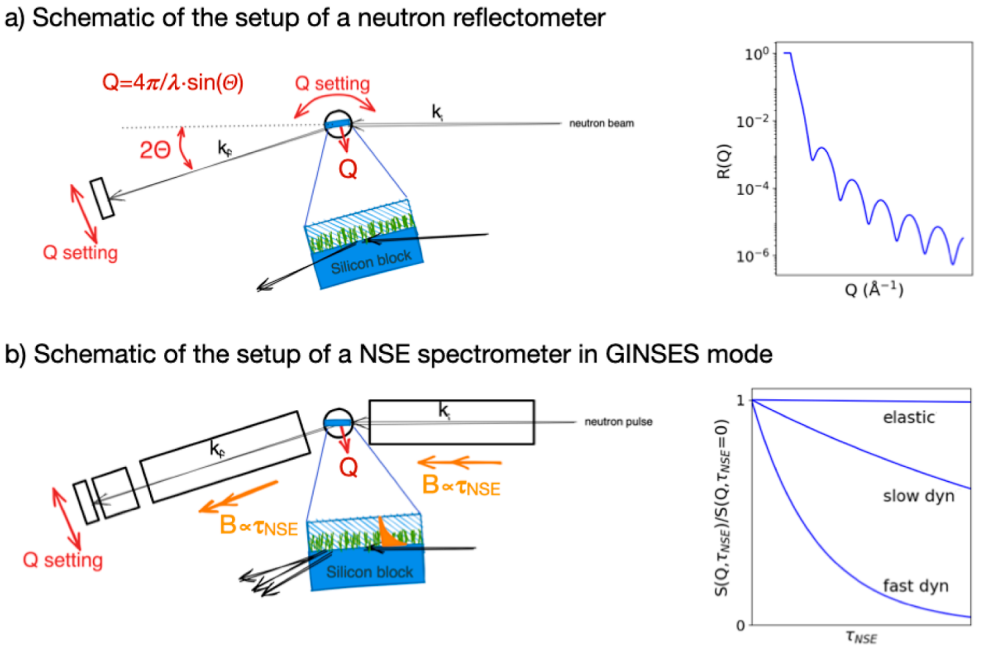

Figure 1. Schematic representations of the experimental setup of (a) a neutron reflectometry (NR) experiment and (b) of a grazing incidence NSE (GINSES) experiment with their typical experimental results. Here, k_i and k_f indicate the wave vectors of the incident and scattered neutrons and Q is the magnitude of the scattering vector. In NSE, the strength B of the magnetic fields before and behind the sample position mainly determines the value of the Fourier time τ_{NSE}. NR provides the scattering length density normal to a planar surface on length scales of nm to some 100 nm. GINSES probes fluctuations in the interface layer during scattering on time scales of the order of 1−100 ns with an evanescent neutron wave. The right side of the schematic representations shows the typical experimental results. In case (a), an oscillating decrease of the reflectivity $R(Q)$ is observed with NR. In case (b), at a fixed Q_z, the intermediate scattering function in semilogarithmic representation (the correlation function in reciprocal space and time) may be observed at different penetration depths of the neutrons into the sample.

side polished, p-type (boron) silicon wafers were purchased from MicroChemicals GmbH (Germany). First, the silicon substrates were cleaned by submersion in acetone and sonicated for 5 min. Afterward, they were rinsed with 2-propanol and dried under a constant stream of nitrogen. They were then functionalized with the silane initiator eBMPUS by immersion in a 0.005 wt % solution (in toluene) at a temperature of −20 °C for 24 h. The thickness of the silane layer of 1.5 nm was determined from ellipsometry measurements.

2.3. SI ATRP of pMEDSAH Brushes. First, silicon substrates were functionalized with the silane initiator eBMPUS by immersion in a 0.005 wt % solution in toluene for 24 h. Afterward, samples were sonicated in toluene for 15 min, rinsed with ethanol, and dried under a stream of nitrogen to remove any excess reactant.

In some cases, a mixture of eBMPUS with trichlorododecylsilane, the so-called "spacer", was used for the surface functionalization in order to reduce the number of active sites and decrease the grafting density. The spacer molecules without the ATRP functionality are chemically similar to the initiator molecules and have approximately the same molecular size. It can therefore be assumed that the initiator and spacer have the same adsorption probability to the substrate and that the ratio of both molecules corresponds to the statistical distribution on the surface. Three different grafting densities were investigated which will be indicated in the text here as σ_0, $\sigma_{0.3}$, and $\sigma_{0.7}$ and refer to spacer/initiator ratio of 0, 30:70, and 70:30, respectively. This variation allows tuning of the mean distance of the anchored chains. Theoretically, σ_0 is the highest grafting density and $\sigma_{0.7}$ the lowest.

Surface-initiated ATRP (SI ATRP) was conducted as described by Qian et al.[34] with the following parameters. A catalyst quantity of 3 mol % was chosen with a catalyst Cu(I)/Cu(II) 1:10. SI ATRP was carried out under an argon atmosphere for 20 h, after which samples were rinsed with 1% sodium chloride solution and deionized water. Samples were then dried with a stream of nitrogen and kept dry until use.

The quantities of the reagents for the SI ATRP were scaled up 6-fold to coat silicon blocks (5 × 8 × 1.5 cm) for neutron scattering experiments. In the following, "dry" experimental conditions refer to a temperature of 20 °C and a relative humidity R_H of 30−50%.

3. METHODS

3.1. Ellipsometry. The thickness of the synthesized pMEDSAH brushes was measured with two different ellipsometers: a nulling ellipsometer (EP3 Nanofilm, Accurion GmbH, Germany) at the University of Michigan for the measurement of brushes swollen in water and a Null-Ellipsometer (Optrel GbR, Germany) at the TU Berlin for the measurement at ambient conditions. Measurements using the EP3 Nanofilm (λ = 532 nm) with the swollen brush layer at room temperature were conducted using the solid/liquid cell (Accurion GmbH, Germany) to determine the swelling ratio of the brush. Further measurements on dry samples were conducted with the Optrel instrument (λ = 532 nm, polarizer-compensator-sample-analyzer setup) at an angle of incidence α_i = 70°, while measurements with the solid/liquid cell called for an α_i = 60°.

3.2. Water Contact Angle. Static water contact angles were measured with deionized water using a contact angle goniometer (Ramé-Hart 200-F1 goniometer). A 2 μL drop of deionized water was deposited on the brush samples. Analysis of the contact angle was performed with the DROPimage Advanced software (Ramé-Hart Instrument Co.).

3.3. Electrokinetic Measurements. Streaming current measurements were performed with an electrokinetic analyzer SurPASS 3 (Anton Paar GmbH, Graz, Austria) for surface testing of materials with automatic zeta potential analysis. The clamping cell was used. During the measurement, the samples were fixed to the holder with a cross-section of 10 × 10 mm^2. The surface zeta potential ζ of the samples was measured in a 1 mM KCl solution at different pH values. The pH of these aqueous electrolytes was adjusted with 0.05 mol/L HCl and 0.05 mol/L KOH, respectively. The fundamental Helmholtz−Smoluchowski dependence for evaluating the ζ potential

https://doi.org/10.1021/acsapm.4c02879
ACS Appl. Polym. Mater. 2025, 7, 5807−5819

from streaming current measurements is given by eq 1, which relates electrokinetic phenomena to the zeta potential[35]

$$\zeta = \frac{\mathrm{d}I_{str}}{\mathrm{d}\Delta p}\frac{\eta}{\epsilon_{rel}\epsilon_0}\frac{L}{A_c} \quad (1)$$

Here, the measured streaming current coupling coefficient $\mathrm{d}I_{str}/\mathrm{d}\Delta p$ is related to the cell constant L/A_c of the flow channel, which is the gap between the sample surface and the sample holder. L denotes the length of the rectangular slit channel formed between two planar surfaces, and A_c is its cross-section, $A_c = W \times H$, with W denoting the channel width and H the gap height. Furthermore, η is the viscosity of the electrolyte, ϵ_{rel} is related to the dielectric coefficient of the electrolyte, and ϵ_0 denotes the vacuum permittivity. For dilute aqueous solutions, η and ϵ_{rel} values of water were used. The streaming potential of a bare Si-wafer over a pH range between 2.5 and 8.7 was compared to the streaming potential of pMEDSAH brushes at the same pH with different grafting densities.

3.4. Neutron Reflectometry. Specular neutron reflectivity at the solid/liquid interface provides information about the relation to the thickness and scattering length density (SLD) profile of interfacial structures along the surface normal z. The SLD profile $\rho(z)$ depends on the chemical composition of materials and is defined as the sum of the coherent nuclear scattering lengths b_i of its constituent atoms and their number density $n_i(z)$ so that $\rho(z) = \sum_i b_i n_i(z)$. Reflectivity data are gathered by recording the intensity of reflected neutrons relative to the incident beam as a function of the momentum transfer vector ($Q_z = 4\pi \sin\theta/\lambda$), where θ is the incidence angle and λ is the wavelength of incident neutrons. The variation of reflectivity as a function of momentum transfer $R(Q_z)$ is related to the square modulus of the one-dimensional Fourier transform of the SLD profile ($\rho(Q_z)$) through the relation $R(Q_z) = (16\pi^2/Q_z^2)|\rho(Q_z)|^2$. Recovery of the SLD profile from $R(Q_z)$ is traditionally performed by model fitting, using thin slab models. A typical experimental setup of a neutron reflectometer and a typical reflectivity curve are shown in Figure 1a. The neutron reflectometry measurements on the brushes in different ionic environments were carried out on the FIGARO instrument at the Institute Laue Langevin (ILL, Grenoble, France).[36] The brush-modified substrates were sealed in a solid−liquid sample cell filled with aqueous NaCl and $MgCl_2$ solutions. The sample cells were connected to an HPLC pump, which allowed for remote control of contrast exchange from deuterated to hydrogenated medium. All of the experiments were conducted at 25 °C with a circulating water bath connected to the sample cell for thermal stabilization. The experiments were conducted in reflection-up mode, and the collimation angle was set to 0.631°. Two incident angles, 0.8 and 3.2°, were selected to cover the full q range from 0.01 to 0.35 Å^{-1}. The frame overlap was set to λ = 20 Å and wavelength resolution $\Delta\lambda/\lambda$ = 7%. The D_2O contrast was used for sample alignment.

The thickness of the brushes measured in the GINSES experiment was measured at the V6 instrument of the Helmholtz-Zentrum Berlin (HZB, Berlin, Germany)[37] using its two slit collimation at the fixed wavelength λ = 4.66 Å and $\Delta\lambda/\lambda$ = 2% The brushes were measured in D_2O, NaCl, and $MgCl_2$ solutions in D_2O (0.1 and 1 M) at 25 °C.

3.5. Analysis of Reflectivity Data. For the analysis of the reflectivity data, two different approaches were used. Due to the inherent ambiguity of NR in assigning a SLD profile to the structure, a model-free approach was used in order to determine the structure of the brushes without additional assumptions. Additionally, a more traditional model-based fit assuming that the pMEDSAH brushes have a bimodal density distribution was used. In the model-independent approach (program DIONYSIA),[38] we first perform an indirect Fourier transform (IFT) of the reflectivity curve for estimating the maximum extension of the brush layer, and subsequently within the limits of the found maximum extension, we perform a search through simulated annealing for the polymer volume fraction profile that better describes the experimental reflectivity curve. The algorithm is essentially similar to the b-spline algorithm described in the literature,[39] with the main difference being the concurrent fit of multicontrast data that in principle leads to a less ambiguous model than the one relying on the fit of one contrast alone. The only estimation that is made concerns the scattering length density (SLD) of the polymer, which is set equal to 0.7 × 10^{-6} Å^{-2} and is certainly close to the real value. Additionally, since the extension of the brush layers (at high salt concentrations) is expected to exceed 1000 Å, we limit the fitted Q_z-range below 0.06 Å^{-1}. It should be noted that the characteristic ripples observed in the volume fraction profiles, with length scales of 50−100 Å, are a consequence of the limited spatial resolution resulting from the finite maximum Q_z employed during the fits.

Model-based analysis was performed using the program Anaklasis[40] and by assuming a polydisperse bimodal distribution profile for the brushes according to the equation

$$\phi(z) = \int_{L_1-3\sigma_1}^{L_1+3\sigma_1} \frac{e^{-\left(\frac{x-L_1}{\sqrt{2}\sigma_1}\right)^2}}{\sigma_1\sqrt{2\pi}} \max\left\{\phi_{10}\left[1-\left(\frac{z}{L_1}\right)^{n_1}\right], 0\right\}\mathrm{d}x + \int_{L_2-3\sigma_2}^{L_2+3\sigma_2} \frac{e^{-\left(\frac{x-L_2}{\sqrt{2}\sigma_2}\right)^2}}{\sigma_2\sqrt{2\pi}} \max\left\{\phi_{20}\left[1-\left(\frac{z}{L_2}\right)^{n_2}\right], 0\right\}, \mathrm{d}x \quad (2)$$

where L_1 and L_2 are the extensions, ϕ_{10} and ϕ_{20} the volume fractions of the two brush modes at z = 0, and n_1 and n_2 the profile exponents, respectively. Brush polydispersity is taken into account by assuming a Gaussian extension distribution with associated standard deviations σ_1 and σ_2. The calculations are performed by dividing the brush profile into 50 equally sized slabs with a SLD value calculated after eq 2 and assuming a polymer and solvent SLD equal to 0.7 × 10^{-6} Å^{-2} and 6.35 × 10^{-6} Å^{-2}, respectively. The resulting SLD profile is based on the polymer volume fraction profile perpendicular to the substrate. Note that the same Q_z-range as for the model-independent fits was used.

3.6. Grazing Incidence Neutron Spin Echo Spectroscopy. Grazing incidence neutron spin echo spectroscopy (GINSES) experiments were conducted on the SNS-NSE instrument at the Oak Ridge National Laboratory (ORNL, Tennessee, USA).[41] A neutron prism was used to correct for differences in the scattering depth.[42,43] This is critical when measuring GINSES at a spallation neutron source and, hence, a pulsed neutron source. A wavelength band of 5 Å to 8 Å was chosen, covering a Fourier time τ_{NSE} range between 0.03 and 45 ns in a Q-range between 0.04 and 0.08 Å^{-1} in a single setting of scattering angle for the second arm of the spectrometer.

Similar to dynamic light scattering (DLS), neutron spin echo (NSE) spectroscopy provides the van Hove correlation function in reciprocal space (called the intermediate scattering function $S(Q, \tau_{NSE})/S(Q, 0)$), normalized to the static correlation function. The main difference to DLS is the probed length- and time scale in the nanometer and nanosecond range and the contrast mechanism resulting from the interaction of neutrons with the subatomic particles, depending on the scattering length in the sample instead of the refractive index difference for light. The contrast, as usual in neutron scattering, is expressed as the scattering length density difference. More details on the NSE technique applied to polymer systems can be found in ref 44.

Interface sensitivity is obtained in the present case with the GINSES setup. Figure 1b illustrates the experimental conditions and the typical experimental outcome. The neutron beam is collimated in the lateral direction and enters the reflectometry-type sample cell under a shallow angle α_i below the critical angle of total reflection α_c

$$\alpha_c = \lambda\sqrt{\Delta\rho/\pi} \quad (3)$$

for neutrons between the silicon block and the brush grafted on top of it, surrounded by the D_2O solvent. For a neutron wavelength of λ = 5 Å and a polymer SLD of 0.7 × 10^{-6} Å^{-2} and using a polymer volume fraction of 0.8 in the vicinity of the silicon substrate according to the NR data yields the critical angle α_c = 0.22°. An evanescent intensity distribution $I_{ev}(z)$ is generated at the interface and decays exponentially $I_{ev} \propto \exp(-z/z_{1/e})$ in the sample. The so-called neutron

https://doi.org/10.1021/acsapm.4c02879
ACS Appl. Polym. Mater. 2025, 7, 5807−5819

penetration depth $z_{1/e}$ is a characteristic distance at which I_{ev} has decayed to $I_{ev,max}/e$, which is tuned by changing α_i and $\Delta\rho$ (e.g., by variation of the H_2O/D_2O ratio in the sample). Here we always used maximum contrast with fully deuterated water. The scattered neutrons of the evanescent wave are then detected at a Q-value determined by the angle of the second arm of the neutron spin echo spectrometer. Since this technique inherently has a very small sample volume to be probed, the scattered intensity is also very low and requires long acquisition times at a very stable instrument with a low neutron background, which is the case for the SNS-NSE.

The data $S(Q, \tau_{NSE})$ at a single or a set of Q values were fitted with a single exponential function of the form

$$S(Q, \tau_{NSE}) = (A - A_{bgr}) \times \exp(-\Gamma_c \tau_{NSE}) + A_{bgr} \quad (4)$$

with the signal amplitude A of the sample and the relaxation rate Γ_c of concentration fluctuations inside the sample, which relates to the diffusion constant by $\Gamma_c = D_{app}Q^2$. Depending on length- and time scales, more advanced fitting procedures can be applied, incorporating, e.g., coarse-grained models for the polymer dynamics in solution such as the Zimm model; see, e.g., ref 44, but the results indicate, as shown later, that on the length- and time scales of the present experiment, concentration fluctuations due to thermally excited motions of the polymer chains are the dominant type of dynamics here.

The GINSES data presented here are not corrected by a background subtraction, but instead, the background A_{bgr} is included in the fitting function since the normalization with the different contrasts is not straightforward and small deviations from the true background could result in large additional errors. In our experiment, the brush sample immersed in D_2O and a clean silicon block in contact with D_2O for determining the background contribution were measured under the same conditions. The background signal is nondecaying (showing no dynamics) with a nonzero elastic contribution.

4. RESULTS AND DISCUSSION

4.1. Brush Synthesis on Planar Silicon Oxide Surfaces.

In our study, we explore the effect of low-molecular-weight salts on polysulfobetaine brushes at different grafting densities with neutron reflectometry. To control the brush thickness required for these measurements, we started our study by characterizing the brush thickness as a function of polymerization time for three grafting densities.

Figure 2 displays the increase of the dry thickness of the synthesized pMEDSAH brushes as a function of the polymerization time t_p for the three different grafting densities (σ_0, $\sigma_{0.3}$, and $\sigma_{0.7}$). As it is mainly observed in SI ATRP, the brush thickness grows in a linear dependence on the polymerization time t_p at the beginning of polymerization. As the polymerization proceeds, the brush thickness increases until reaching a constant value due to termination of further chain growth. The plot shows 4 time points: 60, 90, 1200, and 1320 min. Per sample and time point, three ellipsometry measurements on different areas of the sample were conducted. Error bars are included in the graph; however, they are of the size of the symbols. For the lowest grafting density $\sigma_{0.7}$, the linear dependence is clearly visible. Additionally, the data points spread less at large values of t_p which might indicate a rather narrow chain end distribution for this case. The data suggest that with increasing grafting density $\sigma_{0.3}$ to σ_0, the chain end distribution is increasingly widening. For all prepared brushes, the water contact angles were below 50°, which confirmed the hydrophilicity of these brushes as shown in Figures S1 and S2. To estimate the molecular weight M_n of the synthesized brushes, the averages of the grafting density σ determined from the neutron reflectometry measurements on the brushes in salt solution at 1.0 M given in Table 3 were used. We assume that the initial functionalization of the silicon substrates was the same for the types of silicon samples used when the targeted mean grafting density was the same. The thickness of the dry brushes $t_{dry}(t_p)$ was measured with ellipsometry. According to eq 5

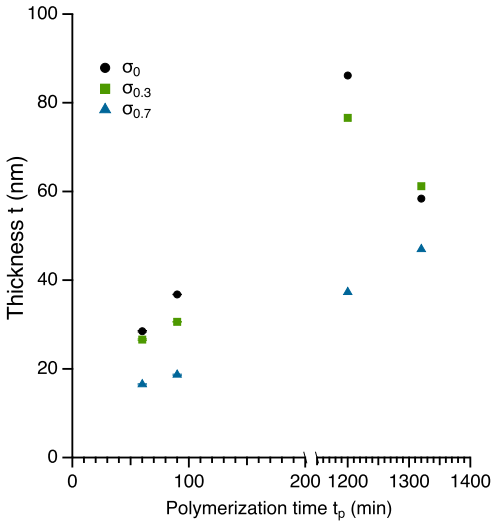

Figure 2. Dry brush thickness t as a function of polymerization time t_p for three different grafting densities σ_0 = 0.21 nm^{-2}, $\sigma_{0.3}$ = 0.16 nm^{-2}, and $\sigma_{0.7}$ = 0.13 nm^{-2} adjusted by the percentage of trichlorododecylsilane molecules in the mixture of eBMPUS + trichlorododecylsilane molecules, with trichlorododecylsilane serving as spacer molecule to lower the grafting density measured via ellipsometry (the linear increase of t vs t_p is due to the break in the x-axis for better visibility).

$$t_{dry} = \frac{M_n \sigma}{N_A \rho_0} \quad (5)$$

a relation is established between the grafting density, the thickness of the dry brush, and the molecular weight M_n of the polymer chains in the brush, with N_A as the Avogadro constant and the mass density of ρ_0 = 1.34 g/cm^3 as given in the literature.[45,46] The resulting molecular weights are given in Table 1. The curve shows the generally observed course of an SI ATRP as described in the literature with an approximately linear increase in the initial phase and a gradual transition to a plateau value, where the longer polymerization times do not lead to any further increase in thickness.[47,48] At the highest value of t_p, the measured dry thickness drops again. This effect was previously described in the literature, where it is termed the super-collapsed state. Possibly, the growing chains collapse

Table 1. Dry Brush Thickness t_{dry} at Polymerization Time t_p = 1200 min in Figure 2[a]

sample	σ (nm^{-2})	t_{dry} (nm)	M_n 10^3 (g/mol)
σ_0	0.21 ± 0.04	86.0 ± 0.5	330 ± 63
$\sigma_{0.3}$	0.16 ± 0.01	77.0 ± 0.5	390 ± 24
$\sigma_{0.7}$	0.13 ± 0.03	37.0 ± 1.0	230 ± 53

[a]At larger t_p, the occurrence of the super collapsed state is assumed to lead to an apparently lower brush thickness. The mean grafting densities σ were estimated from the NR measurements at maximal salt concentration as summarized in Table 3. Values of the molecular weight M_n were estimated from eq 5.

https://doi.org/10.1021/acsapm.4c02879
ACS Appl. Polym. Mater. 2025, 7, 5807−5819

at a certain length due to dipole−dipole interactions between neighboring chains.[47]

4.2. Electrokinetic Measurements. Figure 3 summarizes the results of the zeta potential ζ measurements for the three

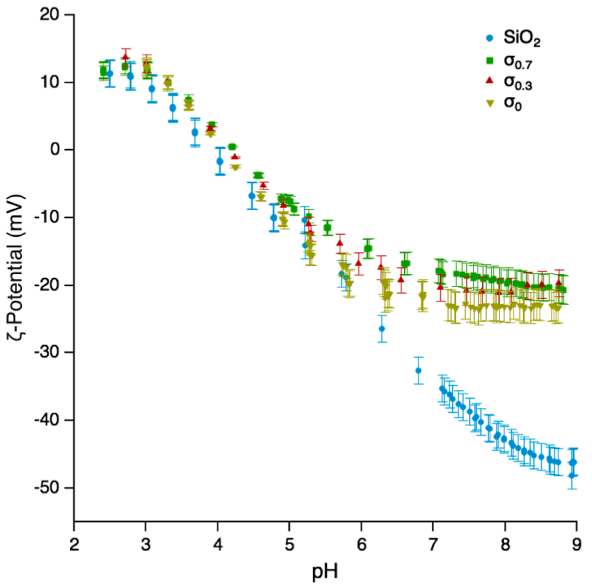

Figure 3. Zeta potential ζ as a function of the solution pH for pMEDSAH brushes with averaged grafting densities σ_0 = 0.21 nm^{-2}, $\sigma_{0.3}$ = 0.16 nm^{-2}, and $\sigma_{0.7}$ = 0.13 nm^{-2} in pure water. For comparison, the data of a plain silicon wafer are shown.

pMEDSAH brushes and compares them to the result obtained with a bare silicon wafer as a reference. The measurements were carried out at pH values ranging from 2.5 to 9. The four curves show a similar course up to pH 6.5 and level off at different plateau values with further increasing pH.

At pH 2.5, the zeta potential of the silicon oxide surface is at +16 mV and drops continuously to −45 mV, where it remains stable for pH > 9. The isoelectric point (IEP) was found at pH 4. In the literature, numerous results from zeta potential measurements with SiO_2 are reported.[6,49] These data cover a range of IEP values from pH 2.5 to pH 4. The reported ζ(pH) curves in the literature are very similar, but the absolute values of ζ show an offset of 10−20 mV. Hence, our result for the reference surface falls well within these reported ranges.

The zeta potential of the three pMEDSAH brushes at pH 2.5 is +15 mV and decreases with increasing pH, until it reaches −20 mV for $\sigma_{0.7}$ and −24 mV for $\sigma_{0.3}$ and σ_0. The isoelectric point at pH 4 is a common observation for neutral polymeric surfaces. The charge formation by adsorption of water ions leads to an equilibrium surface concentration of adsorbed negative hydroxide and positive hydronium ions, which is obtained at pH 4. The fact that an isoelectric point of around pH 4 was found for all samples shows that this mechanism is the dominating mechanism for the surface charge formation. At pH < IEP, the curves are almost identical, while at pH > IEP, differences occur. The surface charge of the plain surface decreases to ζ = −40 mV at around pH 8. The surface charge of the brush-coated surfaces levels off at ζ = −20 mV in neutral and basic solutions. In the region above pH 6, the plateau of the zeta potential at around ζ = −20 mV proves the coverage of the wafer surface. The lower absolute zeta potential values for the modified surface compared to the plain surface at higher pH are caused by the increasing hydrophilicity, causing a lower concentration of adsorbed hydroxide ions on the surface. These findings suggest that independently of the grafting density of the brush, the surface charge is rather low, and the surface polarity is in all three cases rather hydrophilic, as expected for such brush structures. The rather small differences between σ_0, $\sigma_{0.3}$, and $\sigma_{0.7}$ indicate that any possible structural differences between the brushes due to the variation of σ_m have no significant effect on the surface charge density. Moreover, the results suggest that the polymer volume fraction distribution perpendicular to the solid substrate is very similar for all three samples. Polymer brushes are usually polydisperse in terms of chain length and hence brush thickness. This was discussed as a source of distortions to the flow field along the solid substrate which in turn could influence the measured zeta potential.[50]

4.3. Study of the pMEDSAH Brush Structure by Neutron Reflectometry. The pMEDSAH brushes with σ_0, $\sigma_{0.3}$, and $\sigma_{0.7}$ were investigated with neutron reflectometry to explore the effect of the grafting density on the structure of brushes swollen at different ionic strengths. To do so, the brush interfaces were immersed in pure D_2O and NaCl and $MgCl_2$ solutions with concentrations of 0.1 and 1.0 M.

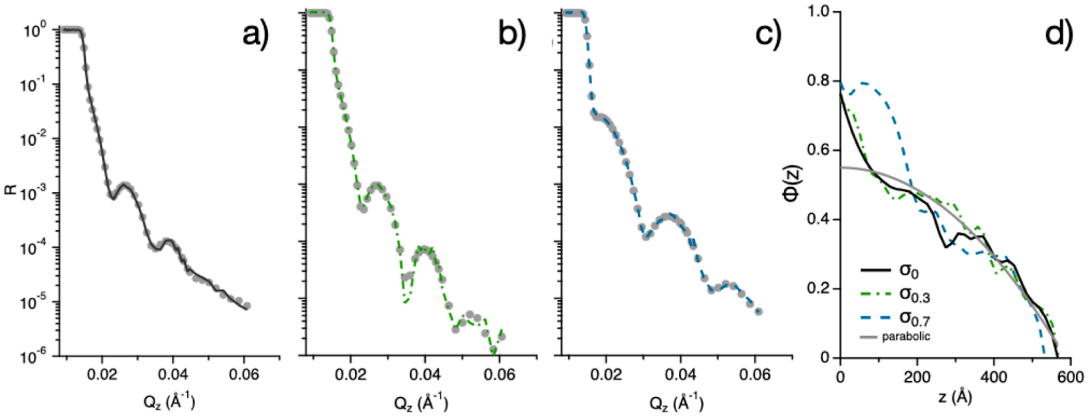

Figure 4. Semilogarithmic representation of the reflectivity curves of pMEDSAH brushes in pure D_2O measured at different spacer/initiator ratios, leading to grafting densities of (a) σ_0, (b) $\sigma_{0.3}$, and (c) $\sigma_{0.7}$. (d) Polymer volume fraction (PVF) profiles $\phi(z)$ obtained from fitting the reflectivity curves (a−c). The accuracy of the polymer volume fractions determined from multiple fitting runs is 5%.

https://doi.org/10.1021/acsapm.4c02879
ACS Appl. Polym. Mater. 2025, 7, 5807−5819

In previous NR studies on zwitterionic brushes, data analysis was based on the assumption of a layered structure of the brushes, accounting for regions of high polymer volume fraction close to the substrate, a "diluted" outer region with a low polymer volume fraction, and an intermediately hydrated region between the two. In addition to the fit with the model of a bimodal brush, we fitted the reflectivity data from the investigated pMEDSAH brushes in a model-free approach as explained in the Methods section. The bimodal-brush model fits where generally successful for the cases where the brushes were not much swollen at low salt conditions of 0.1 M and are depicted in Figures S4 and S5 in the Supporting Information. However, systematically, these fits fail to reproduce the experimental data at higher salt concentrations of 1.0 M, suggesting that the bimodal-brush models cannot describe the actual SLD profiles. The model-free approach was more appropriate to describe the experimental data, and it was therefore applied to analyze all of the experimental data.

4.3.1. Brush Structure in Salt-Free D_2O. Figure 4a−c shows the reflectivity curves of the pMEDSAH brushes with the grafting densities σ_0, $\sigma_{0.3}$, and $\sigma_{0.7}$. All three brushes were immersed in salt-free D_2O. Up to the value of Q_z corresponding to α_c as given by eq 3, total reflection occurs. At this critical edge, the reflectivity R decreases and is followed by two to three distinct Kiessig fringes in the Q_z range of up to 0.06 $Å^{-1}$. This indicates the presence of layers with thicknesses of several 10 nm. Figure 4d shows the resulting polymer volume fraction $\phi(z)$ distributions (PVF) along the normal z to the solid substrate. At first glance, the three curves show the same progression independent of the grafting density. In particular, all three brushes reached a maximum thickness of approximately 55 nm. However, close to the surface, the brush with $\sigma_{0.7}$ shows the highest polymer density of 0.8 up to a thickness of about 20 nm.

The thickness of the D_2O swollen brush h_{wet} was determined 2-fold. On the one hand, it was calculated from the distance ΔQ_z between the Kiessig fringes in the reflectivity curves according to $h_{wet} = 2\pi/\Delta Q_z$. The results are summarized in Table 2. For comparison, the thickness of the dry collapsed brush h_{dry} measured with X-ray reflectometry is also given (the data are shown in Figure S3). These values are in good agreement with a mean dry thickness of these samples of 24 ± 3 nm measured with ellipsometry. The ratio h_{wet}/h_{dry} is a measure of swelling in the pure aqueous environment. Approximately, the brushes are swollen by a factor of 2. This is in good agreement with the observation of swelling ratios of 2−3 for PMPC and PMAPS brushes in salt-free water.[26]

Table 2. Dry Thickness h_{dry} and Thicknesses h_{wet} of the Brushes Swollen with Salt-Free D_2O[a]

sample	σ (nm^{-2})	h_{wet} (nm)	h_{dry} (nm)	h_{wet}/h_{dry}
σ_0	0.21 ± 0.04	53 ± 4	31	1.7 ± 0.1
$\sigma_{0.3}$	0.16 ± 0.01	51 ± 4	22	2.3 ± 0.2
$\sigma_{0.7}$	0.13 ± 0.03	40 ± 3	19	2.1 ± 0.2

[a]From these values, the swelling ratios h_{wet}/h_{dry} were determined.

Additionally, the D_2O swollen brush thickness was determined from the model-free analysis by smoothing the PVF profile with a smoothing routine of the software (Igor Pro 8) and then forming the first derivative. The maximum served as a measure of the thickness of the layer. The results were 32, 38, and 25 nm for σ_0, $\sigma_{0.3}$, and $\sigma_{0.7}$, respectively. Both approaches should yield the same brush thickness for a brush of Gaussian chains with a well-defined brush-D_2O interface. Hence, the difference is a clear indication of a bimodal structure in D_2O with a polymer-rich layer from about 25 to 40 nm near the solid interface.

According to the classic theory of polymer brushes, a parabolic volume fraction profile $\phi(z)$[51]

$$\phi(z) = \phi_0(1 - (z/h^*)^2)) \tag{6}$$

should describe the decrease of the polymer volume fraction $\phi(z)$ with increasing distance z from the confining surface. A fit to the data shown in Figure 4d indicates that in the salt-free case at $z \geq 20$ nm a mean parabolic PVF profile with $\phi_0 = 0.55$ and a maximal thickness of h* = (59 ± 2) nm is a good approximation for all three brushes as theoretically predicted and mostly experimentally observed for neutral brushes. However, at $z \leq 20$ nm, very close to the substrate, $\phi(z)$ is larger than in a parabolic curve of an ideal polydisperse brush of Gaussian chains. This together with the steeper decay of $\phi(z)$ indicates a compaction of the polymer chains near the substrate with a thicker layer in the case of $\sigma_{0.7}$. However, the PVF profiles are very similar and suggest a rather small influence of the grafting density on the brush structure outside the compacted layer. This observation is supported by the results of the electrokinetic measurements.

4.4. Effect of Ionic Strength on the Structure of pMEDSAH Brushes. To study the effect of the ionic strength of additional salt in the aqueous environment on the structure of the pMEDSAH brushes, the samples were immersed in NaCl and $MgCl_2$ solutions, whose ionic strengths are important to mimic biologically relevant aqueous electrolyte solutions. Additionally, due to their mono- and divalent cations, the same monovalent anion equal salt concentration yields different ionic strengths.

4.4.1. Brush Swelling in NaCl Solution. From the analysis of the reflectivity curves measured for pMEDSAH brushes in NaCl solution (Figures S6 and S7) of the Supporting Information, the volume fraction profile shown in Figure S6 was obtained. There, the fits according to a layered model and the model-free fits are compared. Figure 5 summarizes the resulting PVF distributions $\phi(z)$, in particular, in graph (a), the PVFs obtained with σ_0 are plotted; in graph (b), the PVFs for $\sigma_{0.3}$ are given; and graph (c) summarizes the results for $\sigma_{0.7}$. The areas below the curves agree rather well with each other, except for the case of 0.1 M NaCl, which disagrees strongly by 40% from the other curves in Figure 5a. However, as can be seen, the adsorbed amount varies within 25% of the mean value, as shown in Table 3. The brush thickness was determined from the model-free analysis by smoothing the polymer volume fraction profile with a smoothing routine to reduce the effect of the unevenness in the profiles resulting from the fits and then forming the first derivative. The maxima serve as a measure of the corresponding thickness, h_{max}, of the layer.

From the maximum thickness h_{max} found in the PVFs, a swelling ratio h_{max}/h_{dry} was calculated to compare the brush extension due to the presence of NaCl and $MgCl_2$. Table 3 summarizes the resulting values of the stretched brushes for NaCl as well as $MgCl_2$ at both measured concentrations of 0.1 and 1.0 M compared to the salt-free case. As h_{max} increases, the profile significantly changes from parabolic to bimodal. Besides this, the profiles at σ_0 show a decrease of $\phi_0(z = 0)$ from 0.8

https://doi.org/10.1021/acsapm.4c02879
ACS Appl. Polym. Mater. 2025, 7, 5807−5819

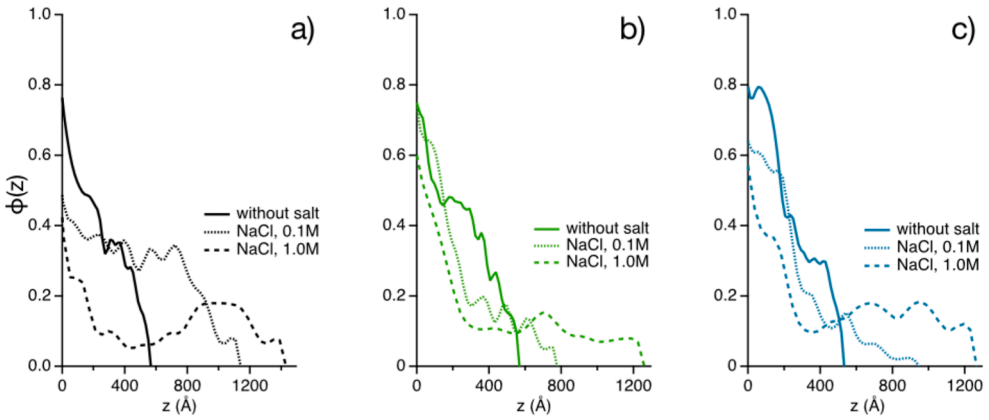

Figure 5. Polymer volume fraction profiles of the brushes shown in images (a) σ_0, (b) $\sigma_{0.3}$, to (c) $\sigma_{0.7}$, calculated from the fits to the reflectivity data of the brushes in NaCl solutions of different concentrations. The accuracy of the polymer volume fractions determined from multiple fitting runs is 5%.

Table 3. Results of Model-Free Fits to the Reflectivity Curves from the Brushes in Aqueous NaCl and $MgCl_2$ Solutions[a]

sample	c_{NaCl} (mol/L)	c_{MgCl_2} (mol/L)	Γ (mg/m^2)	h_{max} (nm)	h_{max}/h_{dry}	N	M_n 10^3 (g/mol)	σ (nm^{-2})	d (nm)
σ_0	0.1	0	36.0 ± 2.0	56 ± 1	1.9				
$\sigma_{0.3}$	0.1	0	25.0 ± 1.3	67 ± 2	3				
$\sigma_{0.7}$	0.1	0	23.4 ± 1.2	86 ± 5	4.5				
σ_0	1.0	0	22.7 ± 1.1	130 ± 2	4	520	144 ± 3	0.170	2.4
$\sigma_{0.3}$	1.0	0	28.1 ± 1.4	100 ± 5	4.5	400	112 ± 6	0.160	2.5
$\sigma_{0.7}$	1.0	0	24.7 ± 1.2	92 ± 2	4.8	370	103 ± 2	0.151	2.6
σ_0	0	0.1	36.0 ± 1.8	57 ± 2	3.6				
$\sigma_{0.3}$	0	0.1	31.2 ± 1.6	55 ± 2	2.5				
$\sigma_{0.7}$	0	0.1	31.0 ± 1.6	45 ± 2	2.4				
σ_0	0	1.0	26.1 ± 1.3	87 ± 5	3.2	348	100 ± 6	0.254	2.0
$\sigma_{0.3}$	0	1.0	21.1 ± 1.1	100 ± 3	4.6	410	113 ± 4	0.158	2.5
$\sigma_{0.7}$	0	1.0	22.9 ± 1.1	135 ± 2	7	540	150 ± 3	0.104	3.1

[a]Values of the adsorbed quantities Γ, maximal brush thickness h_{max}, and the swelling ratio h_{max}/h_{dry} are given. Molecular weight M_n, grafting density σ, and the mean distance $d = 1/\sqrt{(\sigma)}$ between the grafting sites were estimated from the results for the highest salt concentrations, assuming the brushes to be maximally swollen in that case.

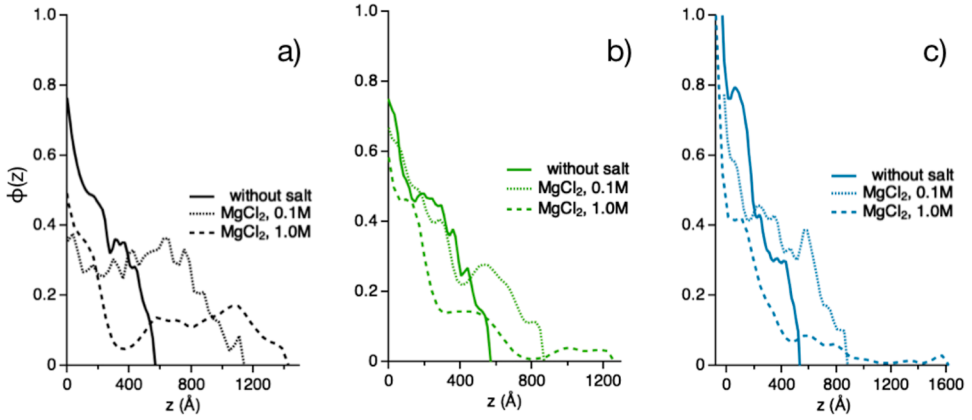

Figure 6. Polymer volume fraction profiles of the brushes shown in images: (a) grafting densities σ_0, (b) $\sigma_{0.3}$ to (c) $\sigma_{0.7}$, calculated from the fits to the reflectivity data of the brushes in $MgCl_2$ solutions of different concentrations. The accuracy of the polymer volume fractions determined from multiple fitting runs is 5%.

down to 0.5, indicating a higher polymer dilution close to the substrate. At medium z (around 40−80 nm), $\phi(z)$ is larger when the pMEDSAH chains are surrounded by a NaCl solution. This indicates a significant stretching of the polymer chains away from the surface. With $\sigma_{0.3}$ and $\sigma_{0.7}$, no such drop of ϕ_0 was observable.

4.4.2. Brush Swelling in $MgCl_2$ Solution. In Figure 6, $\phi(z)$ profiles obtained from fitting the NR data (Figures S8 and S9) measured with the investigated pMEDSAH brushes immersed in deuterated $MgCl_2$ solutions are shown.

The comparison between the PVF profiles of σ_0, $\sigma_{0.3}$, and $\sigma_{0.7}$ shows similar features to the PVF profiles measured with

https://doi.org/10.1021/acsapm.4c02879
ACS Appl. Polym. Mater. 2025, 7, 5807−5819

NaCl solutions. Again at σ_0, the value of ϕ_0 decreases from 0.75 to 0.48 at increasing concentration of $MgCl_2$, while the pMEDSAH chains reconfigure at medium distances ≈40−60 nm from the interface. Here, the profile of $\phi(z)$ changes again to bimodal.

However, for $\sigma_{0.3}$ and $\sigma_{0.7}$, both the values of ϕ_0 and the course of $\phi(z)$ change less than in the case when the brushes were immersed in NaCl solution. At $\sigma_{0.3}$ and $\sigma_{0.7}$, the values of h_{max} are slightly larger than with NaCl, and the course of $\phi(z)$ shows minor differences for the different salt concentrations for $MgCl_2$ compared with the courses obtained with NaCl.

4.4.3. Comparison. Figure 7 summarizes the brush thicknesses for the ionic strengths measured with NR (Tables 2 and 3). The ionic strength I is the product of the molar concentration and charge number of the ions summed for all ions. The open symbols refer to the aqueous $MgCl_2$ solution, and solid symbols indicate salt-free water at $I = 0$ and aqueous NaCl solution otherwise. When compared to the salt-free case with a wet brush thickness of 50−60 nm (Figure 4), the increase of the maximal brush thickness is visible for all grafting densities. The increase from I = 1 mol/L to 3 mol/L is minimal and approaches a limit value around 130 nm, which yields a maximal stretching by a factor of approximately 3 to 5 compared with the dry thickness. Such swelling factors were also previously determined in NR measurements for PMAPS brushes in aqueous NaCl solution.[22] A further increase in the ionic strength might therefore not lead to further stretching of the polymer chains. Considering the maximal stretching of the polymer chains in the brushes, the stretching of the chains in the presence of the divalent cation Mg^{2+} seems to be less pronounced. It was reported in the literature that the presence of divalent cations may induce dehydration and interchain bridging which would result in a reduction of the chain stretching.[27,29] The brush thicknesses at 1.0 M NaCl and 1.0 M $MgCl_2$ were assumed to be close to the maximal stretching of the polymer chains. They were used to estimate the mean degree of polymerization N and the mean molecular weight M_n of the chains. This approach was chosen to take into account the variation in brush thicknesses depending on the required substrate size and to avoid technically challenging approaches, such as degrafting of polymer chains. The estimations were based on a value of 0.25 nm for the length of the repeat unit in the chain and its molecular weight of 279 g/cm^3.[45,48] Furthermore, using eq 5 with the calculated molecular weights yields values for the grafting density σ. To consider experimental uncertainties, the results of the measurements at 1.0 M for both salts were taken into account in determining σ. Averaged values of σ_0 = 0.21 nm^{-2}, $\sigma_{0.3}$ = 0.16 nm^{-2}, and $\sigma_{0.7}$ = 0.13 nm^{-2} were obtained and used for further considerations. This corresponds to a mean distance $d = 1/\sqrt{\sigma}$ between the grafting points of 2.2, 2.5, and 2.8 nm. These values confirm the semidilute brush regime at all three grafting densities. Despite the large variation in the spacer/initiator ratio, only a small effective variation of σ was obtained. Possibly, the interchain association causes an apparently low reduction in the case of a spacer/initiator ratio of 70:30 but confirms the semidilute regime of the brushes. Based on tabulated bond lengths, the length of the side arms carrying the sulfonate and quaternary ammonium groups can be estimated to be approximately 1.3 nm. The mean distance between the grafting sites of 2−3 nm suggests that certain conformational bending is required to neutralize the charged groups in interchain interactions, which then leads to a polymer-rich layer in the vicinity of the surface.

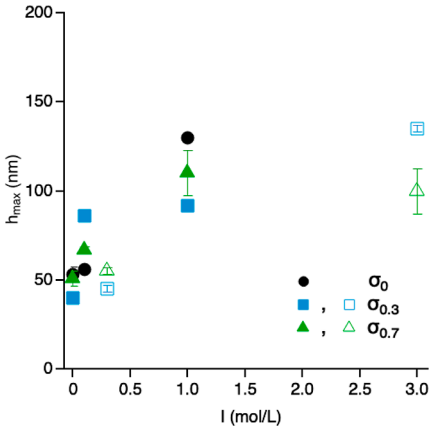

Figure 7. Maximal brush thickness h_{max} as summarized in Table 3 as a function of ionic strength I for pMEDSAH brushes with averaged grafting densities σ_0 = 0.21 nm^{-2}, $\sigma_{0.3}$ = 0.16 nm^{-2}, and $\sigma_{0.7}$ = 0.13 nm^{-2}. The open symbols refer to measurements with $MgCl_2$; solid symbols are either with NaCl or without salt (I = 0) (see also Table 2).

A comparison of the PVF profiles $\phi(z)$ in Figures 5 and 6 indicates similar stretching of the brushes. However, the observed brush thicknesses indicate that in the presence of the divalent cation Mg^{2+}, the thicknesses are lower and the antipolyelectrolyte effect is less pronounced when compared to the presence of Na^+. This is suggested by the higher values of h_{max} in the outer region of the brushes. Only at 1.0 M would more elongated chains occur as more interchain associations are broken than at the lower concentration. Speculatively, it could be that the ions could then diffuse deeper into the brush. Moreover, the chosen values of the grafting density influenced the observed brush thickness in the dry and water-swollen states, as is known for neutral brushes but showed only a minor influence on the brush structure at different values of the ionic strength.

4.5. Near Surface Dynamics in pMEDSAH Brushes. The dynamics of this thick polymer brush with a maximal achievable grafting density of σ_0 at the interface was studied with GINSES.

GINSES requires a sample thickness of >100 nm so that sufficient neutrons from the evanescent intensity distribution can be scattered on the sample and then be deflected. Therefore, a brush thickness of 100−200 nm was aimed for. At these layer thicknesses, no more Kiessig fringes can be observed, and $R(Q_z)$ falls off as a smooth curve. The thickness of the brush prepared for GINSES was estimated using the model-free approach and a layer model for a polydisperse brush (Figure S10).

The relaxation rates Γ_c in the intermediate scattering functions (see eq 4) measured with polymer brushes are either small (observed as an incomplete decay within the experimentally accessible Fourier time window) or large (decay to zero after a few ten nanoseconds) and contain information on concentration fluctuations at low $Q < 1/\xi_{blob}$ which is diffusion of blobs of size ξ_{blob}. Figure 8 illustrates the dynamics probed with GINSES; the size of a blob is given by the distance of the grafting sites of neighboring polymer chains. A grafted chain can be interpreted as a chain of blobs, and a brush is a close packing of these blobs. In an ideal brush with

https://doi.org/10.1021/acsapm.4c02879
ACS Appl. Polym. Mater. 2025, 7, 5807−5819

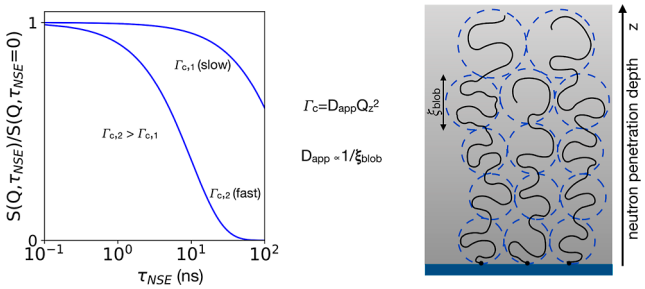

Figure 8. Scheme of dynamics in a planar polymer brush seen with NSE at a fixed value of Q_z. The observed decay of the intermediate scattering function shown in semilogarithmic representation yields a relaxation rate of the concentration fluctuations Γ_c, which decays either fast or slow. Since $\Gamma_c = D_{app}Qz^2$ and $D_{app} \propto 1/\xi_{blob}$, the value of Γ_c is small when the related dynamics $\Gamma_c/Q_z \propto 1/\xi_{blob}$ measures fluctuations of rather large concentration blobs with size ξ_{blob}. A fast decay indicates the fluctuations of smaller-sized blobs.

uniform chain length, all blobs have the same size. However, in a polydisperse brush, the blob size increases with increasing distance from the grating surface, and hence, thickness-dependent dynamics should occur. At high $Q > 1/\xi_{blob}$, the dynamics inside a blob is probed. Here, the segmental dynamics of a polymer chain dominates the signal. Hence, dependent on the penetration depth of the neutrons into the brush and dependent on Q, a significant decrease of the intermediate scattering function should occur. Only if in parts of the brush these motions are hindered or suppressed, does a constant time plateau A_{bgr} occur or is there a very slow dynamic that only falls off on time scales outside the experimentally accessible time range. The brush was measured at an angle of incidence $\alpha_i = 1.0°$, leading to a virtually infinite neutron penetration depth $z_{1/e} \gg h_{max}$ since $\alpha_i \gg \alpha_c$. Figure 9 exemplary shows the intermediate scattering functions $S(Q, \tau_{NSE})$ for three Q values $Q = 0.04$ Å^{-1}, $Q = 0.05$ Å^{-1}, and $Q = 0.07$ Å^{-1}. All three measurements show a flat course of $S(Q, \tau_{NSE})$ within the time window of observation τ_{NSE}. The precision is somehow already limited by the statistics at large Fourier times. Moreover, in GINSES measurements, conventional background correction and reference measurements need to be modified, as discussed in previous work.[32,52] The inherently low signal intensity decreases with increasing Q, and hence, measurements were not reasonable at larger Q, which would provide more local information. The GINSES experiments are therefore limited to observations of large-scale dynamics such as density fluctuations at length scales larger than the thermal blob size ξ_{th}. Segmental dynamics inside this blob are difficult to access for brushes in GINSES experiments. The flat course of $S(Q, \tau_{NSE})$ indicates the absence of density fluctuations with large fluctuation amplitudes for these brushes. A small signal amplitude $A-A_{bgr}$ of a few percent is superimposed at a high elastic background of $A_{bgr} \approx 70-80\%$ of the total signal amplitude A. Considering the limitations, an upper limit for the relaxation rates of $\Gamma_c \leq 10^{-3}$ ns^{-1} can be estimated. Following the simplified Alexander–de Gennes blob picture for brushes, from the dispersion relation of a diffusional motion $\Gamma_c = D_{app}Qz^2$, the lower limit for the radius of the corresponding spherical blobs ξ_{blob} of 40 nm can be estimated by applying the Stokes–Einstein-type equation $D = k_BT/(6\pi\eta\xi_{blob})$ for a temperature of 20 °C in D_2O at $Q = 0.05$ Å^{-1}. Compared to typical blob sizes of a few nanometers estimated for neutral brushes, this large value indicates long-range correlations of the pMEDSAH chains. This suggests that correlated fluctuations extend over several individual chains. Furthermore, it is reasonable to assume that the mean fluctuation amplitude is low due to the strong coupling of the neighboring chains. Possibly, bound water and the counterion distribution with its hydration shells also act as a medium with an effectively high apparent viscosity. That would also dampen the fluctuations of the polymer chains in the brush. A comparison with earlier measurements on PNIPAM brushes and PEG brushes shows clear differences.[32,52] A clear mobility of the outer areas of the brushes can be observed in the neutral brushes. In addition to the electrostatic coupling of the zwitterionic chains, the stronger binding of the hydrate shells can also contribute to the damping of the mobility of the chain segments. This clear difference in the hydrate shells was demonstrated by NMR measurements.[53] In a recent study using dynamic light scattering on polyzwitterionic chains in salt-free and dilute salt solutions, it was observed that polyzwitterionic polymer chains in salt-free conditions relax more slowly to thermal excitation than in a dilute salt solution.[20]

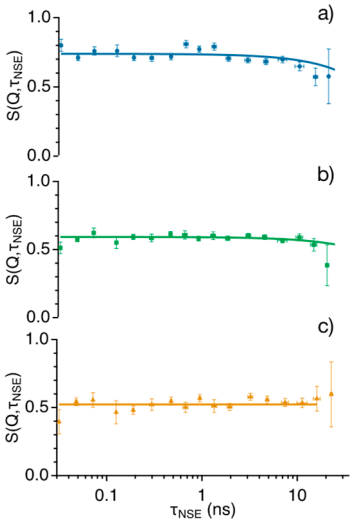

Figure 9. Semilogarithmic representation of the intermediate scattering functions measured for brush σ_0 in pure D_2O at an angle of incidence $\alpha_i = 1°$ and hence virtually infinite neutron penetration depth at (a) $Q = 0.04$ Å^{-1}, (b) $Q = 0.05$ Å^{-1}, and (c) $Q = 0.07$ Å^{-1}. The course of the intermediate scattering functions is rather flat without a significant decay, which indicates a rather damped dynamics in the system.

5. CONCLUSIONS

In this study, we explored the influence resulting from the antipolyelectrolyte effect of salt type (monovalent and divalent) and ionic strength on the structure of semidilute zwitterionic polysulfobetaine brushes with varying grafting densities. The brush structure was investigated with neutron reflectometry, and the measured reflectivity curves $R(Q_z)$ were analyzed in both a bimodal-structure model and a model-free fitting approach to extract the polymer volume fraction profiles $\phi(z)$. The polysulfobetaine brushes are swollen by a factor of approximately 2 in salt-free water. At increasing ionic strength, the brushes swell and the maximum brush thickness increases by a factor of 3–5 compared to the dry state. At the highest ionic strengths, the stretching approaches a plateau value. This

https://doi.org/10.1021/acsapm.4c02879
ACS Appl. Polym. Mater. 2025, 7, 5807–5819

finding was independent of the grafting density. The investigated pMEDSAH brushes show a tendency to form a diffuse, approximately bimodal structure in the presence of mono- and divalent cations. A combined investigation of these structural properties with NR and AFM could provide additional insights into the protein adhesion resistance of such zwitterionic brushes.

GINSES was used to measure the chain dynamics in the brushes to investigate how the chain dynamics of zwitterionic brushes in the salt-free state differ from the dynamics of neutral brushes in a good solvent. We found that the interchain interactions due to dipole−dipole, charge−charge, and also charge−dipole interactions lead to an extensive suppression of thermally excited fluctuations of the segments in the nanometer and nanosecond range and conclude that in this partially swollen state, the brush structure is rather chain-rigid. Further investigations can lead to an understanding of the chain and segment dynamics of such systems in the presence of electrolytes and possibly explore the transition from the dynamics of rather rigid chains to a stronger influence of concentration fluctuations on the observed dynamics. Moreover, it would be interesting to relate such future findings to the well-understood dynamics of neutral brushes and to investigate their possible contribution to the protein repellence of these systems.

■ ASSOCIATED CONTENT

Supporting Information

The Supporting Information is available free of charge at https://pubs.acs.org/doi/10.1021/acsapm.4c02879.

Plot of pMEDSAH brush thickness and related water contact angles as a function of the spacer content, fitted reflectivity curves of the pMEDSAH brushes in solutions of NaCl and $MgCl_2$, and fitted reflectivity curves of the pMEDSAH brushes used in the GINSES measurements (PDF)

■ AUTHOR INFORMATION

Corresponding Author

Stefan Wellert − *Department of Chemistry, Technische Universität Berlin, 10623 Berlin, Germany;* orcid.org/0000-0001-7050-0957; Phone: +49 (0)30 31424958; Email: s.wellert@tu-berlin.de; Fax: +49 (0)30 31426602

Authors

Judith Witte − *Department of Chemistry, Technische Universität Berlin, 10623 Berlin, Germany*

Alexandros Koutsioubas − *Jülich Centre for Neutron Science at Heinz Maier-Leibnitz Zentrum, Forschungszentrum Jülich, 85747 Garching, Germany;* orcid.org/0000-0001-9417-5108

Samantha Micciulla − *MODI, Laboratoire Interdisciplinaire de Physique, Centre National de la Recherche Scientifique, 38402 Saint Martin d'Hères, France; Institut Laue-Langevin, 38000 Grenoble, France*

Laura Roxana Stingaciu − *NScD, SNS, Oak Ridge National Laboratory, Oak Ridge National Laboratory, Oak Ridge, Tennessee 37830, United States;* orcid.org/0000-0003-2696-5233

Mariano Andrés Paulin − *Helmholtz Zentrum Berlin für Energie und Materialien, 14109 Berlin, Germany; Laboratorio Argentino de Haces de Neutrones, Centro Atómico Bariloche, CNEA, San Carlos de Bariloche R8402AGP, Argentina*

Margarethe Dahl − *Department of Chemistry, Technische Universität Berlin, 10623 Berlin, Germany;* orcid.org/0000-0003-3993-9050

Christian Fettkenhauer − *Anton Paar Germany GmbH, 73760 Ostfildern-Scharnhausen, Germany*

Joerg Lahann − *Institut für Funktionelle Grenzflächen, Karlsruhe Institute of Technology, 76344 Eggenstein-Leopoldshafen, Germany*

Olaf Holderer − *Jülich Centre for Neutron Science at Heinz Maier-Leibnitz Zentrum, Forschungszentrum Jüllich, 85747 Garching, Germany;* orcid.org/0000-0001-6746-7965

Complete contact information is available at: https://pubs.acs.org/10.1021/acsapm.4c02879

Notes

The authors declare no competing financial interest.

■ ACKNOWLEDGMENTS

The dynamics part of this research used resources at the Spallation Neutron Source, a DOE Office of Science User Facility operated by the Oak Ridge National Laboratory. This work is based upon experiments performed at the Heinz Maier-Leibnitz Zentrum (MLZ), Garching, Germany. Neutron reflectometry measurements were performed at the ILL, Grenoble, and the HZB, Berlin. We thank Luca Silvi for his assistance with the measurements at the HZB. Parts of the laboratory work were conducted in the Lahann Lab at the University of Michigan. Water contact angle measurements were conducted in the PSI Lab at the University of Michigan. Therefore, we would like to thank Professor Lahann and Professor Tuteja for providing resources. The author S.M. thanks the PSCM platform for granting access to the infrastructure for sample preparation.

■ REFERENCES

(1) Laschewsky, A.; Rosenhahn, A. Molecular design of zwitterionic polymer interfaces: searching for the difference. *Langmuir* **2019**, *35*, 1056−1071.

(2) Higaki, Y.; Kobayashi, M.; Takahara, A. Hydration state variation of polyzwitterion brushes through interplay with ions. *Langmuir* **2020**, *36*, 9015−9024.

(3) Karthäuser, J. F.; Kopecz, R.; Schönemann, E.; Martinez Guajardo, A.; Laschewsky, A.; Rosenhahn, A. Spacer Effects in Sulfo- and Sulfabetaine Polymers on Their Resistance against Proteins and Pathogenic Bacteria. *Adv. Mater. Interfaces* **2024**, *11*, 2300873.

(4) Mi, L.; Jiang, S. Integrated antimicrobial and nonfouling zwitterionic polymers. *Angew. Chem., Int. Ed.* **2014**, *53*, 1746−1754.

(5) He, Q.; Qiao, Y.; Medina Jimenez, C.; Hackler, R.; Martinson, A. B.; Chen, W.; Tirrell, M. V. Ion Specificity Influences on the Structure of Zwitterionic Brushes. *Macromolecules* **2023**, *56*, 1945−1953.

(6) Kopsch, F.; Drechsler, A.; Priebs, M.; Caspari, A.; Müller, A.; Lentz, S.; Friedrichs, J.; Synytska, A. Zwitterionic Polymer Brushes and Core-Shell Particles Based thereon for Control of Biofouling. *Macromol. Chem. Phys.* **2023**, *224* (9), 2200454.

(7) Khakzad, F.; Dewangan, N. K.; Li, T.; Safi Samghabadi, F.; Herrera Monegro, R.; Robertson, M. L.; Conrad, J. C. Fouling resistance and release properties of poly(sulfobetaine) brushes with varying alkyl chain spacer lengths and molecular weights. *ACS Appl. Mater. Interfaces* **2023**, *15*, 2009−2019.

(8) Jiang, S.; Cao, Z. Ultralow-Fouling, Functionalizable, and Hydrolyzable Zwitterionic Materials and Their Derivatives for Biological Applications. *Adv. Mater.* **2010**, *22*, 920−932.

(9) Song, X.; Man, J.; Qui, Y.; Wang, J.; Liu, J.; Li, R.; Zhang, Y.; Li, J.; Li, J.; Chen, Y. High-density zwitterionic polymer brushes exhibit robust lubrication properties and high antithrombotic efficacy in blood-contacting medical devices. *Acta Biomater.* **2024**, *178*, 111−123.
(10) Karthäuser, J. F.; Gruhn, D.; Martínez Guajardo, A.; Kopecz, R.; Babel, N.; Stervbo, U.; Laschewsky, A.; Viebahn, R.; Salber, J.; Rosenhahn, A. In vitro biocompatibility analysis of protein-resistant amphiphilic polysulfobetaines as coatings for surgical implants in contact with complex body fluids. *Front. Bioeng. Biotechnol.* **2024**, *12*, 1403654.
(11) Krishnan, S.; Weinman, C. J.; Ober, C. K. Advances in polymers for anti-biofouling surfaces. *J. Mater. Chem.* **2008**, *18*, 3405−3413.
(12) Xie, Q.; Pan, J.; Ma, C.; Zhang, G. Dynamic surface antifouling: mechanism and systems. *Soft Matter* **2019**, *15*, 1087−1107.
(13) Jin, H.; Tian, L.; Bing, W.; Zhao, J.; Ren, L. Bioinspired marine antifouling coatings: status, prospects, and future. *Prog. Mater. Sci.* **2022**, *124*, 100889.
(14) Higaki, Y.; Nishida, J.; Takenaka, A.; Yoshimatsu, R.; Kobayashi, M.; Takahara, A. Versatile inhibition of marine organisms settlement by zwitterionic polymer brushes. *Polym. J.* **2015**, *47*, 811−818.
(15) Paschke, S.; Lienkamp, K. Polyzwitterions: From Surface Properties and Bioactivity Profiles to Biomedical Applications. *ACS Appl. Polym. Mater.* **2020**, *2*, 129−151.
(16) Kitano, H.; Kawasaki, A.; Kawasaki, H.; Morokoshi, S. Resistance of zwitterionic telomers accumulated on metal surfaces against nonspecific adsorption of proteins. *J. Colloid Interface Sci.* **2005**, *282*, 340−348.
(17) Ikada, Y. Blood-compatible polymers. *Adv. Polym. Sci.* **1984**, *57*, 103−140.
(18) Schlenoff, J. B. Z. Zwitteration: Coating Surfaces with Zwitterionic Functionality to Reduce Nonspecific Adsorption. *Langmuir* **2014**, *30*, 9625−9636.
(19) Georgiev, G. S.; Kamenska, E. B.; Vassileva, E. D.; Kamenova, I. P.; Georgieva, V. T.; Iliev, S. B.; Ivanov, I. A. Self-assembly, antipolyelectrolyte effect, and nonbiofouling properties of polyzwitterions. *Biomacromolecules* **2006**, *7*, 1329−1334.
(20) Liu, Z.; Keum, J. K.; Li, T.; Kumar, R.; Chen, J.; Hong, K.; Wang, Y.; Sumpter, B. G.; Advincula, R.; Sumpter, B. G. Anti-polyelectrolyte and polyelectrolyte effects on conformations of polyzwitterionic chains in dilute aqueous solutions. *PNAS Nexus* **2023**, *2*, pgad204.
(21) Kobayashi, M.; Terayama, Y.; Kikuchi, M.; Takahara, A. Chain dimensions and surface characterization of superhydrophilic polymer brushes with zwitterion side groups. *Soft Matter* **2013**, *9*, 5138−5148.
(22) Kobayashi, M.; Ishihara, K.; Takahara, A. Neutron reflectivity study of the swollen structure of polyzwitterion and polyeletrolyte brushes in aqueous solution. *J. Biomater. Sci., Polym. Ed.* **2014**, *25*, 1673−1686.
(23) Sakamaki, T.; Inutsuka, Y.; Igata, K.; Higaki, K.; Yamada, N. L.; Higaki, Y.; Takahara, A. Ion-Specific Hydration States of Zwitterionic Poly(sulfobetaine methacrylate) Brushes in Aqueous Solutions. *Langmuir* **2019**, *35*, 1583−1589.
(24) Huang, C.; Li, Y.; Krause, J. B.; Brault, N. D.; Jiang, S. Internal architecture of zwitterionic polymer brushes regulates nonfouling properties. *Macromol. Rapid Commun.* **2012**, *33*, 1003−1007.
(25) Mondarte, E. A. Q.; Shi, Y.; Koh, X. Q.; Feng, X.; Daniel, D.; Zhang, X. X.; Yu, J. Unveiling the Layered Structure of Sulfobetaine Polymer Brushes through Bimodal Atomic Force Microscopy. *Macromolecules* **2023**, *56*, 5001−5009.
(26) Kobayashi, M.; Terayama, Y.; Hino, M.; Ishihara, K.; Takahara, A. Characterization of swollen structure of high-density polyelectrolyte brushes in salt solution by neutron reflectivity. *J. Phys.: Conf. Ser* **2009**, *184*, 012010.
(27) Song, X.; Man, J.; Zhang, X.; Wang, J.; Zhang, Y.; Li, J.; Du, J.; Chen, Y.; Li, J.; Chen, Y. Atomistic insights into the ionic response and mechanism of antifouling zwitterionic polymer brushes. *Small* **2025**, *21*, 2406233.
(28) Reitenbach, J.; Geiger, C.; Wang, P.; Vagias, A.; Cubitt, R.; Schanzenbach, D.; Laschewsky, A.; Papadakis, C. M.; Müller-Buschbaum, P. Effect of magnesium salts with chaotropic anions on the swelling behavior of PNIPAM thin films. *Macromolecules* **2023**, *56*, 567−577.
(29) Yu, J.; Jackson, N. E.; Xu, X.; Morgenstern, Y.; Kaufman, Y.; Ruths, M.; De Pablo, J. J.; Tirrell, M. Multivalent counterions diminish the lubricity of polyelectrolyte brushes. *Science* **2018**, *360*, 1434−1438.
(30) Hu, N.; Lin, L.; Metwalli, E.; Bießmann, L.; Philipp, M.; Hildebrand, V.; Laschewsky, A.; Papadakis, C. M.; Cubitt, R.; Zhong, Q.; Müller-Buschbaum, P. Kinetics of Water Transfer Between the LCST and UCST Thermoresponsive Blocks in Diblock Copolymer Thin Films Monitored by In Situ Neutron Reflectivity. *Adv. Mater. Interfaces* **2022**, *10*, 2201913.
(31) Kreuzer, L. P.; Widmann, T.; Geiger, C.; Wang, P.; Vagias, A.; Heger, J. E.; Haese, M.; Hildebrand, V.; Laschewsky, A.; Papadakis, C. M.; Müller-Buschbaum, P. Salt-dependent phase transition behavior of doubly thermoresponsice poly(sulfobetaine)-based diblock copolymer films. *Langmuir* **2021**, *37*, 9179−9191.
(32) Witte, J.; Krause, P.; Kyrey, T.; Dahl, A. M.; Lutzki, J.; Schmidt, B. V. K. J.; Ganeva, M.; Koutsioubas, A.; Holderer, O.; Wellert, S. Grazing Incidence Neutron Spin Echo Study of Poly(N-isopropylacrylamide) Brushes. *Macromolecules* **2020**, *53*, 1819−1830.
(33) Witte, J.; Kyrey, T.; Lutzki, J.; Dahl, A. M.; Kühnhammer, M.; Klitzing, R. v.; Holderer, O.; Wellert, S. Looking inside Poly (N-Isopropylacrylamide) Microgels: Nanomechanics and Dynamics at Solid−Liquid Interfaces. *ACS Appl. Polym. Mater.* **2021**, *3*, 976−985.
(34) Qian, X.; Villa-Diaz, L. G.; Kumar, R.; Lahann, J.; Krebsbach, P. H. Enhancement of the propagation of human embryonic stem cells by modifications in the gel architecture of PMEDSAH polymer coatings. *Biomaterials* **2014**, *35*, 9581−9590.
(35) Lorenzetti, M.; Gongadze, E.; Kulkarni, M.; Junkar, I.; Iglič, A. Electrokinetic Properties of TiO2 Nanotubular Surfaces. *Nanoscale Res. Lett.* **2016**, *11*, 378.
(36) Campbell, R.; Wacklin, H.; Sutton, I.; Cubitt, R.; Fragneto, G. FIGARO: The new horizontal neutron reflectometer at the ILL. *Eur. Phys. J. Plus* **2011**, *126* (11), 107.
(37) Trapp, M. V6: The Reflectometer at BER II. *J. Large-Scale Res. Facil.* **2017**, *3*, A114.
(38) Koutsioubas, A. Model-independent recovery of interfacial structure from multi-contrast neutron reflectivity data. *J. Appl. Crystallogr.* **2019**, *52*, 538−547.
(39) Pedersen, J. Model-Independent Determination of the Surface Scattering-Length-Density Profile from Specular Reflectivity Data. *J. Appl. Crystallogr.* **1992**, *25*, 129−1452.
(40) Koutsioubas, A. *anaklasis*: a compact software package for model-based analysis of specular neutron and X-ray reflectometry data sets. *J. Appl. Crystallogr.* **2021**, *54*, 1857−1866.
(41) Ohl, M.; et al. The spin-echo spectrometer at the Spallation Neutron Source (SNS). *Nucl. Instrum. Methods Phys. Res., Sect. A* **2012**, *696*, 85−99.
(42) Frielinghaus, H.; Holderer, O.; Lipfert, F.; Monkenbusch, M.; Arend, N.; Richter, D. Scattering depth correction of evanescent waves in inelastic neutron scattering using a neutron prism. *Nucl. Instrum. Methods Phys. Res., Sect. A* **2012**, *686*, 71−74.
(43) Frielinghaus, H.; Gvaramia, M.; Mangiapia, G.; Jaksch, S.; Ganeva, M.; Koutsioubas, A.; Mattauch, S.; Ohl, M.; Monkenbusch, M.; Holderer, O. New tools for grazing incidence neutron scattering experiments open perspectives to study nano-scale tribology mechanisms. *Nucl. Instrum. Methods Phys. Res., Sect. A* **2017**, *871*, 72−76.
(44) Richter, D.; Monkenbusch, M.; Arbe, A.; Colmenero, J. *Neutron Spin Echo in Polymer Systems*; Springer, 2005; pp 1−221.
(45) Starck, P.; Mosse, W. K. J.; Nicholas, N. J.; Spiniello, M.; Tyrrell, J.; Nelson, A.; Qiao, G. G.; Ducker, W. A. Surface Chemistry

and Rheology of Polysulfobetaine-Coated Silica. *Langmuir* **2007**, *23*, 7587−7593.
(46) Yang, Z.; Zhang, S.; Tarabara, V. V.; Bruening, M. L. Aqueous swelling of zwitterionic poly(sulfobetaine methacrylate) brushes in the presence of ionic surfactants. *Macromolecules* **2018**, *51*, 1161−1171.
(47) Cheng, N.; Brown, A. A.; Azzaroni, O.; Huck, W. T. S. Thickness-Dependent Properties of Polyzwitterionic Brushes. *Macromolecules* **2008**, *41*, 6317−6321.
(48) Yang, W.; Chen, S.; Cheng, G.; Vaisocherová, H.; Xue, H.; Li, W.; Zhang, J.; Jiang, S. Film Thickness Dependence of Protein Adsorption from Blood Serum and Plasma onto Poly(sulfobetaine)-Grafted Surfaces. *Langmuir* **2008**, *24*, 9211−9214.
(49) Bousse, L.; Mostarshed, S.; van der Shoot, B.; de Rooij, N.; Gimmel, P.; Göpel, W. Zeta potential measurements of Ta_2O_5 and SiO_2 thin films. *J. Colloid Interface Sci.* **1991**, *147*, 22−32.
(50) Zimmermann, R.; Freudenberg, U.; Schweiß, R.; Küttner, D.; Werner, C. Hydroxide and hydronium ion adsorption-A survey. *Curr. Opin. Colloid Interface Sci.* **2010**, *15*, 196−202.
(51) Milner, S. T.; Witten, T. A.; Cates, M. E. A Parabolic Density Profile for Grafted Polymers. *Europhys. Lett.* **1988**, *5*, 413−418.
(52) Wellert, S.; Hübner, J.; Boyaciyan, D.; Ivanova, O.; von Klitzing, R.; Soltwedel, O.; Holderer, O. Near surface dynamics of layers of non-cross-linked and cross-linked polymer architectures at solid planar surfaces. *Colloid Polym. Sci.* **2018**, *296*, 2005−2014.
(53) Wu, J.; Lin, W.; Wang, Z.; Chen, S.; Chang, Y. Investigation of the hydration of nonfouling material poly (sulfobetaine methacrylate) by low-field nuclear magnetic resonance. *Langmuir* **2012**, *28*, 7436−7441.

https://doi.org/10.1021/acsapm.4c02879
ACS Appl. Polym. Mater. 2025, 7, 5807−5819